Biphasic $0.8BaTiO_3/0.2Ni_{(1-x)}Co_xFe_2O_4$ nanopowders by *in situ* sol-gel synthesis

D. M. S. Ceron[1], C. P. F. Perdomo[1], S. A. Eliziario[1], M. J. Kaufman[2], R. H. G. A. Kiminami[3]*

[1]Federal University of São Carlos, Graduate Program in Materials Science and Engineering, São Carlos, SP, Brazil

[2]Colorado School of Mines, Department of Metallurgical and Materials Engineering, Golden, CO, USA

[3]Federal University of São Carlos, Department of Materials Engineering, 13565-905, São Carlos, SP, Brazil

Abstract

Nanopowders of the $0.8BaTiO_3/0.2Ni_{(1-x)}Co_xFe_2O_4$ (x= 0, 0.25, 0.5, 0.75, and 1) were synthesized by the *in situ* sol-gel method using poly(acrylic acid) (PAA1800) as a chelating agent. The synthesis developed using PAA1800 ensured the simultaneous crystallization of two phases. The results provided a reliable method for producing biphasic nanopowders in all the compositions of Co-Ni-ferrite with an average particle size of less than 50 nm with a potential application in lead-free magnetoelectric particulate composites. The XRD results indicated the formation of only $BaTiO_3$ and $Ni_{(1-x)}Co_xFe_2O_4$ phases, verifying that there was no interdiffusion between the perovskite $BaTiO_3$ and spinel Co-$NiFe_2O_4$ phases during the crystallization phase. A detailed analysis of the crystalline structures was conducted to quantify the phases using the Rietveld method, and thus ensure the success of the *in situ* sol-gel synthesis.

Keywords: *in situ* sol-gel, $0.8BaTiO_3/0.2Ni_{(1-x)}Co_xFe_2O_4$, nanopowders, biphasic system.

INTRODUCTION

Nanopowders of biphasic systems containing a ferroelectric phase and (ferri)ferromagnetic phase are generally used in particulate magnetoelectric composite systems, belonging to the group of multiferroic materials. Magnetoelectric multiferroic materials are those that exhibit properties derived from the coupling of electric and magnetic ordering parameters, whose main feature is the phenomenon to induce electrical polarization by applying an external magnetic field and also induce magnetic polarization by applying an external electric field [1]. Properties that allow expanding the spectrum of technological applications, mainly in spintronics and electronic devices, such as the control of magnetization through an electric field can optimize devices with smaller sizes and integrated properties [1-3]. In the case of composite magnetoelectric materials, the property is originated from the elastic-mechanical coupling between a (ferri)ferromagnetic (magnetostrictive) phase and a ferroelectric (piezoelectric) phase [3]. Usually, the constituent phases of these two-phase systems are ferromagnetic-magnetostrictive materials such as ferrites, in their pure or doped phase, especially cobalt ferrite ($CoFe_2O_4$) and nickel ferrite ($NiFe_2O_4$) for presenting a higher magnetostriction coefficient λ_m= -110x10^6 and -26x10^6, respectively [4].

For the ferroelectric-piezoelectric phase, especially in the last decade, researchers have focused on the development of lead-free materials due to the RoHS regulation (2002/95/EC) concerning the restriction of hazardous substances, which deals with the restriction of using certain hazardous substances in electronic devices, including lead. Examples of recently used ferroelectric-piezoelectric systems are found: $K_{0.5}Na_{0.5}Nb_2O_3$ (KNN) [5, 6], (x)$Bi_{0.5}Na_{0.5}TiO_3$-(1-x) $Bi_{0.5}K_{0.5}TiO_3$ (BNT-BKT) [7], $Sr_xBa_{1-x}Nb_2O_6$ (SBN) [8], and $BaTiO_3$ [9-11], the latter having been widely explored as a ferroelectric phase in magnetoelectric composites, mainly due to its chemical stability. Thus, to ensure the adequate performance of the magnetoelectric particulate composite, it is essential that the particulate composite presents high densification, control and homogeneity of grain sizes, chemical and stoichiometric control of the interfaces, and, above all, a high level of dispersion of the constituent phases in the biphasic system in the powder state and consequently in the sample conformed [1-3].

The standard method of synthesis of this biphasic system is the mechanical mixture of the constituent crystalline phases of interest, where each phase is synthesized separately using one of several different synthesis routes that include conventional solid-state reactions [12] and chemical routes [13, 14], with the difficulty of ensuring a high degree of homogeneity of phase dispersion, generating a notable percolation of the most electrically conductive phase (ferrite), which leads to a deficit in the magnetoelectric behavior of the composite. For this, new synthesis methods to obtain these two-phase systems have been developed recently, as is the case of *in situ* synthesis, which consists of the simultaneous crystallization of the two phases during a single heat treatment step [13, 14]. Thus, synthesis by this method is an opportunity to obtain both phases simultaneously starting from a single solution and producing

*https://orcid.org/0000-0002-0885-6191

a homogeneous distribution of multiple phases. Based on these arguments, it turns out that the *in situ* synthesis using the sol-gel method may offer an opportunity to produce nanoparticulate biphasic $0.8BaTiO_3/0.2Ni_{(1-x)}Co_xFe_2O_4$ in a single step with greater homogeneity of the powder mixture in less time and lower energy consumption in the complete cycle. It is also of considerable interest to produce nanoscale composite powders in which the phases may be closely linked at the nanoscale as this should represent the best connectivity between phases.

During sol-gel synthesis, poly(acrylic acid) (PAA) can be used as a chelating agent. The chelating agent is used to ensure more homogeneous dispersion of the metal cations. An important characteristic of chelating agents is their functionality, which is believed to significantly help the formation of cross-linked polymeric resins. Cross-linked resins, in turn, may ensure that cations are mixed more homogeneously and may also reduce the tendency for segregation during the heat treatment of ceramic powders. For example, some authors reported the size and morphology of $NiFe_2O_4$ particles synthesized when using PAA as the chelating agent during sol-gel synthesis [15, 16] while others reported the synthesis of ultrafine $Ni_{(1-x)}Co_xFe_2O_4$ (with x= 0, 0.25, 0.5, 0.75, and 1) particles using the sol-gel method [17]. The objective of this work was to synthesize a nanosized $0.8BaTiO_3/0.2Ni_{(1-x)}Co_xFe_2O_4$ diphase system using the poly(acrylic acid) (PAA1800) as the chelating agent in the *in situ* sol-gel method for the application in particulate magnetoelectric composites.

EXPERIMENTAL

The nanopowders of the biphasic system $0.8BaTiO_3/0.2Ni_{(1-x)}Co_xFe_2O_4$ (x= 0, 0.25, 0.5, 0.75, and 1) were synthesized via *in situ* sol-gel synthesis according to the following procedure. Stoichiometric amounts of cobalt acetate ($CoC_4H_6O_4.4H_2O$, Aldrich, 99%), nickel acetate ($NiC_4H_6O_4.4H_2O$, Aldrich, 99%), and iron nitrate [$Fe(NO_3)_3.9H_2O$, Merck, 99%] were dissolved in distilled water. In addition, barium acetate ($BaC_4H_6O_4.4H_2O$, Aldrich, 99%) was dissolved in a 0.5 M nitric acid (HNO_3, Merck, 65%) aqueous solution and tetraethyl orthotitanate ($C_8H_{20}O_4Ti$, Merck, 95%) was dissolved in 2-methoxiethanol ($CH_3OCH_2CH_2OH$, Aldrich, 99.8%). These solutions were then mixed together at 40 ºC to form homogeneous transparent solutions. The poly(acrylic) acid (PAA, Aldrich, Mw=1800), PAA1800, a chelating agent was dissolved in distilled water under constant stirring and then added to the single solution with all-metal cations to form the final solution. Ammonium hydroxide was slowly added to this solution while stirring constantly until a pH ~9.5 was achieved. The resultant solution was evaporated at 60 °C for ~24 h until a translucent brown gel was obtained. For the preparation of the gel precursor, the molar ratio of PAA1800 to total metal ion content was 0.5. The dry gel was then decomposed at 600 °C. At this stage, exothermic decomposition of the gel took place, and the temperature was measured using an infrared pyrometer (RAYMM2M2VF1V, Raytek) using data logger software (DataTemp Multidrop, Raytek) as shown in Fig. 1. After decomposition, the dry gel was turned into powder, which was then heat-treated at 800 °C for 1 h.

Figure 1: Temperature measurement during pyrolytic decomposition reactions of the dry gel: 1) pyrometer; and 2) sample.

The $BaTiO_3$ and $Ni_{(1-x)}Co_xFe_2O_4$ powders were prepared separately following the same PAA1800 sol formation procedure described above in order to compare the possible distortion of unit cells in Co-Ni-ferrite and the biphasic system. The thermal decomposition behavior of the dry gel was followed by TG/DSC (thermogravimetry/differential scanning calorimetry) using a thermal analyzer (STA 409, Netzsch). X-ray powder diffraction (XRD) data were collected on a diffractometer (Rotaflex RU200B, Rigaku) with CuKα radiation with Ni filter at room temperature. XRD data were collected from 10-80° (2θ), with a step size of 0.02° and 3 s/step. Structural refinement of all XRD data was analyzed using the Topas Academic computing program to quantify the phases via the Rietveld method. The particle size was also estimated from the specific surface area (BET method) results, considering phase density and assuming that particles were spherical, using a BET system (ASAP 2020, Micromeritics) and nitrogen. X-ray fluorescence chemical characterization was performed with an X-ray fluorescence spectrometer (Series EDX, Shimadzu). Finally, the particle

size and morphology of the nanopowders were characterized by scanning and transmission electron microscopy (SEM and TEM) using a Philips XL30 FEG and Philips CM12 TEM operating at 120 kV, respectively.

RESULTS AND DISCUSSION

The xerogel obtained after drying from the gel formed by the aqueous solution of metal cations and PAA1800 had a translucent brown color with no precipitates, indicating its homogeneity in composition. The effectiveness of using PAA1800 as a chelating agent in the gel was due to the chemical bonding of the cations to the polymeric chain [18]. According to some authors [15, 19], the presence of functional groups (e.g., COOH) in the PAA might help to form a chelate with mixed metal cations resulting in a homogeneously dispersed sol.

The decomposition of the gel precursor was investigated by thermal analysis of a dried gel of $0.8BaTiO_3/0.2Ni_{(1-x)}Co_{(x)}Fe_2O_4$. The thermogravimetric and differential scanning calorimetric (TG-DSC) data from all composition samples were similar and indicated that the behavior during the burning of the xerogel precursor did not depend on the Ni/Co ratio in the gel. Fig. 2 shows the TG-DTG/DSC curves of the $0.8BaTiO_3/0.2Ni_{0.5}Co_{0.5}Fe_2O_4$ composition as a representative curve of all the compositions studied in this work because for all case compositions, the thermal analysis behavior was similar, and the curves indicated that there were four temperature ranges associated with weight loss, namely, 50-150 °C (region I), 150-250 °C (region II), 250-550 °C (region III), and 700-750 °C (region IV). The first weight loss (about 8%) occurred in the range of 50-150 °C (region I) and corresponded to the removal of superficial and structural solvents from the gel precursor accompanied by an endothermic peak with a maximum at 96 °C in the DSC and DTG data. Such behavior has been observed in other systems previously [18, 19]. The smaller weight loss (about 3%) in the range of 150-250 °C (region II) was associated with the decomposition of some intermediate compounds, such as ammonium nitrate with a peak in the gel decomposition at ~200 °C. In this case, the gel swelled due to the evaporation of some of the products including residual water (H_2O) and the decomposition of ammonium nitrate [$NH_4(NO_3)$] to N_2 and N_2O, as observed in other systems [18, 20, 21]. The most significant weight loss of about 60% occurred between 250 and 550 °C (region III) and was the result of two exothermic reactions, the first peak located at 350 °C, associated with the formation of the intermediate phase $BaCoO_3$ as observed in the XRD pattern in Fig. 3. An intermediate phase helped in the formation of $BaTiO_3$ as reported in the work of Motta et al. [22] and the second peak located at 390 °C corresponded to oxidation and decomposition of organic constituents in the gel precursor. The pyrolysis decomposition behavior was supported by the observation of the gel during heating on the hot plate. Specifically, the data from the infrared pyrometer system indicated that the temperature was approximately 600 °C when the programmed temperature of the hot plate was 400 °C consistent with the relatively large exotherm peak in Fig. 2. Likewise, gel burning was also observed during the pyrolysis reaction in this temperature range. Finally, the small weight loss (~3%) between 700-750 °C appeared to be related to the final decomposition of $BaCO_3$ for complete crystallization pathways of $BaTiO_3$ when using acetates as starting reagents; this was accompanied by a small endothermic peak with the maximum at 711 °C in the DSC data. According to the DTG curve, all physical-chemical events presented by the sample as a function of temperature were associated with mass loss. Similar behavior was reported previously in other ceramic systems [23-25]. The last stage began at about 750 °C and, while there was no significant weight loss observed above this temperature, there were few small endothermic events on the DSC curve that are believed to be associated with the complete crystallization and growth of the $0.8BaTiO_3/0.2Ni0_{.5}Co_{0.5}Fe_2O_4$ biphasic powders; similar behavior was reported by previous authors [23].

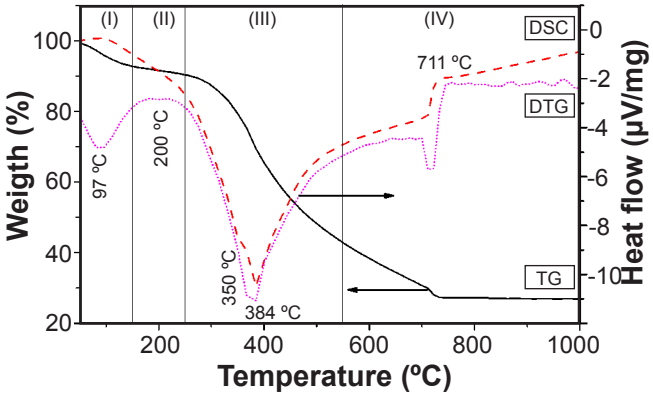

Figure 2: Thermogravimetry and differential scanning calorimetry (TG-DTG/DSC) curves of $0.8BaTiO_3/0.2Ni_{0.5}Co_{0.5}Fe_2O_4$ composition of xerogel.

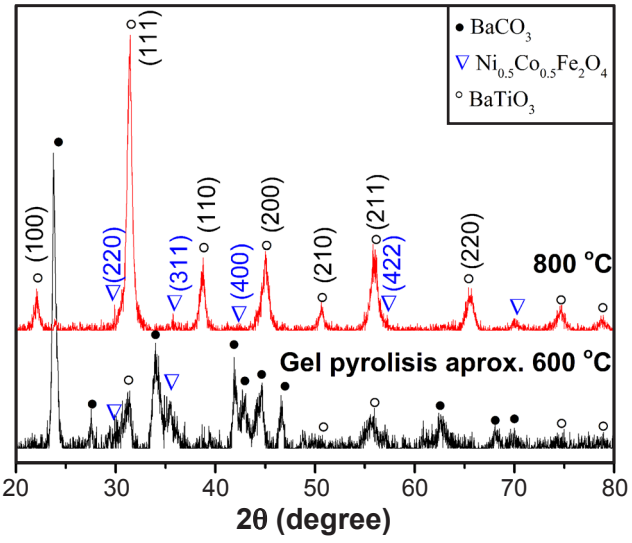

Figure 3: XRD patterns of $0.8BaTiO_3/0.2Ni_{0.5}Co_{0.5}Fe_2O_4$ powder after pyrolysis of the gel precursor at 600 °C and after heat treatment at 800 °C for 1 h.

Upon completion, the pyrolysis product at approx. 600 °C, according to pyrometry, as described in the experimental procedure section, appeared as a fluffy dark brown powder and the X-ray diffraction pattern in Fig. 3 was consistent with $BaCO_3$ (ICSD 45-1471) forming as an intermediate phase along with some peaks from $BaTiO_3$ (ICSD 75-214) and $Ni_{0.5}Co_{0.5}Fe_2O_4$ (ICDD 79-1744), as inferred from the TG/DSC curves in Fig. 2. It could be observed that at the pyrolysis temperature (approx. 600 °C), the crystallization process of $BaTiO_3$ (ICSD 75-214) and $Ni_{0.5}Co_{0.5}Fe_2O_4$ (ICDD 79-1744) phases began. In the dry gel annealed at 800 °C for 1 h (Fig. 3), both $BaTiO_3$ and $Ni_{0.5}Co_{0.5}Fe_2O_4$ phases were observed. The heat treatment temperature of the sample was consistent with the crystallization peak of $BaTiO_3$ above 750 °C based on the DSC-TG data. The results of XRD analysis in Fig. 4 revealed that the *in situ* synthesis of $0.8BaTiO_3/0.2Ni_{(1-x)}Co_xFe_2O_4$ (x= 0, 0.25, 0.5, 0.75, and 1) system was achieved successfully at 800 °C for 1 h; these temperature and holding time conditions were considerably lower than those typically reported in the literature for conventional solid-state reactions, which use around 1200 °C and 3 or 4 h [10], which indicated that the *in situ* sol-gel method using PAA1800 as a chelating agent can be used to quickly obtain the $BaTiO_3$ and $Ni_{(1-x)}Co_xFe_2O_4$ biphasic system in a single reaction step. The main diffraction peaks for the $BaTiO_3$, namely (100), (111), (110), (200), (210), (211), and (220), can be assigned to the perovskite structure, cubic Pm-3m spatial group (ICSD 01-75-0214), with a maximum diffraction intensity for the (111) plane. For the cubic spinel $Ni_{(1-x)}Co_xFe_2O_4$, spatial group Fd-3m with Ni-ferrite (ICSD 89-4927) and Co-ferrite (ICSD 22-1086) phases, the peak intensities of crystalline planes (220), (311) (maximum diffraction peak), (400), and (422), evident in XRD patterns (Fig. 4), were apparently lower compared to the BZT phase. This was due to the atomic scattering factor (f), which depends proportionally on the atomic number (Z), and the scattering factor defined as ($f^2=I/I_{cor}$); for the $BaTiO_3$ phase, the $f^2=11.11$, which is greater than for $NiFe_2O_4$ and $CoFe_2O_4$, which $f^2= 4.83$ and 2.70, respectively.

The Rietveld refinement technique was used to provide a quantitative analysis of the crystalline structure and phase proportion for each ceramic biphasic powder obtained *in situ*: $0.8BaTiO_3/0.2Ni_{(1-x)}Co_xFe_2O_4$. The lattice parameters in Table I were calculated based on the Rietveld refinement using the Topas Academic computing program and were used to verify the incorporation of cobalt cation into the $Ni_{(1-x)}Co_xFe_2O_4$. The refined crystallographic data were in good agreement with the structural parameters in standard ICSD files. In other words, the goodness of fit (χ^2) values were relatively below about 2%, which is considered acceptable according to the basic principles of having a χ^2 less than 4% and an R_{wp} of less than 20% [26]. In the same way, it was essential to compare the lattice parameters of each $BaTiO_3$ and $Ni_{(1-x)}Co_xFe_2O_4$ phase in the biphasic system with each single-phase obtained separately in order to verify both the unwanted entry of Fe^{3+}, Co^{2+}, and Ni^{2+} ions into the perovskite structure, as well as the distortion of the cubic spinel of nickel ferrite by effectively incorporating cobalt ions. The analysis results of phases obtained separately are shown in Table II.

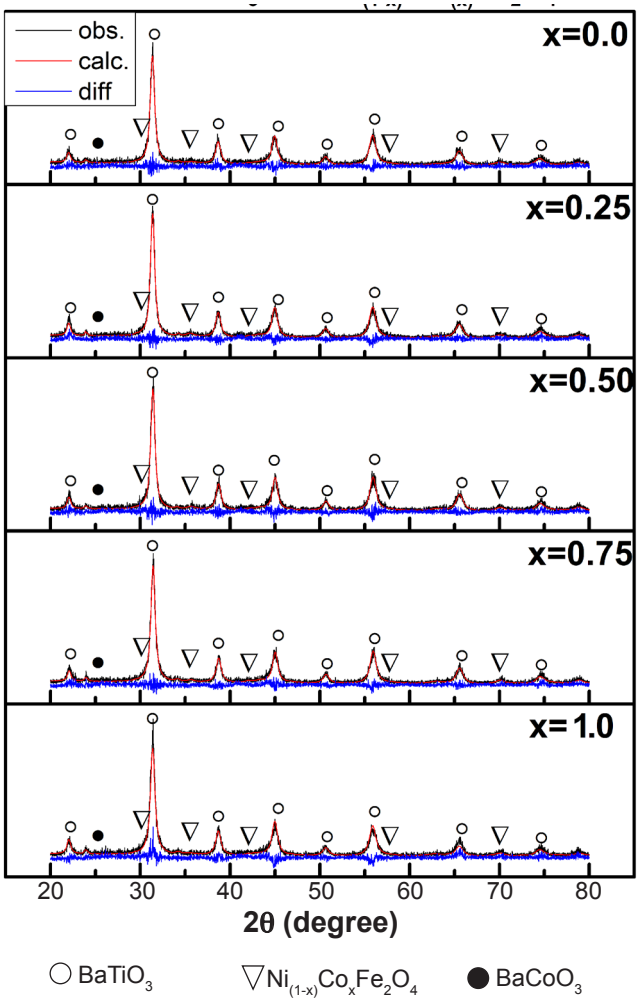

Figure 4: XRD patterns of the $0.8BaTiO_3/0.2Ni_{(1-x)}Co_xFe_2O_4$ composites with x= 0, 0.25, 0.5, 0.75, and 1 showing the results of the Rietveld refinement.

As can be observed from results in Table I and Fig. 4, $BaTiO_3$ was the major phase in all nanopowders, in which $BaCO_3$ was present as a secondary phase. The insertion of cobalt ions into the Ni-ferrite was observed to decrease the barium carbonate presence concomitant to the increase in the Co-ferrite phase formation. In other words, the phase fraction of Ni-ferrite was found to decrease with the simultaneous increase in the content of $BaCO_3$. This indicated that the crystallization of $CoFe_2O_4$ was more favorable than that of $NiFe_2O_4$ during the *in situ* synthesis of $0.8BaTiO_3/0.2Ni_{(1-x)}Co_xFe_2O_4$ following the synthesis protocol used in this work. From the analysis of the network parameters of the two-phase nanopowders $0.8BaTiO_3/0.2(Ni_{(1-x)}Co_xFe_2O_4$ and $CoFe_2O_4)$, and $BaTiO_3$ and $Co_xNi_{(1-x)}Fe_2O_4$ powders obtained separately, shown in Tables I and II, respectively, the expansion of the Ni-ferrite unit cell can be observed by adding the cobalt ion, which was attributed to the difference in the ionic radius between

Table I - Structural parameters by Rietveld refinement analysis, BET surface area, and average particle diameter for the $0.8BaTiO_3/0.2Ni_{(1-x)}Co_xFe_2O_4$ synthesized by *in situ* sol-gel synthesis.

Composition, x (mol%)	$Ni_{(1-x)}Co_xFe_2O_4$ phase (mol%)	$BaTiO_3$ phase (mol%)	$BaCO_3$ phase (mol%)	$BaTiO_3$ lattice parameter (Å)	$Ni_{(1-x)}Co_xFe_2O_4$ lattice parameter (Å)	BET surface area (m^2/g)	Average particle diameter (nm)
0	11.04	83.43	5.53	4.0289	8.3319	15.1±0.1	~67
0.25	9.86	85.16	4.98	4.0279	8.3373	18.5±0.3	~55
0.50	17.11	79.18	3.71	4.0265	8.3469	16.0±0.1	~63
0.75	20.27	76.15	3.58	4.0281	8.3615	13.5±0.1	~77
1.00	24.38	72.47	3.15	4.0275	8.3759	10.6±0.6	~98

Table II - Structural parameters by Rietveld refinement analysis, BET surface area, and average particle diameter for the $BaTiO_3$ and $Ni_{(1-x)}Co_xFe_2O_4$ (x= 0, 0.25, 0.5, 0.75 and 1) phases synthetized separately.

Sample	Lattice parameter (Å)	BET surface area (m^2/g)	Average particle diameter (nm)
$BaTiO_3$	4.0169	15.8±0.1	~63
$NiFe_2O_4$	8.3366	21.0±0.2	~45
$Ni_{0.75}Co_{0.25}Fe_2O_4$	8.3413	22.6±0.1	~42
$Ni_{0.50}Co_{0.50}Fe_2O_4$	8.3479	16.1±0.1	~58
$Ni_{0.25}Co_{0.75}Fe_2O_4$	8.3731	13.0±0.4	~86
$CoFe_2O_4$	8.3891	12.6±0.2	~89

Co^{2+} (0.82 Å), Ni^{2+} (0.78 Å), and Fe^{3+} (0.67 Å) [16], a similar behavior presented both in the two-phase system and in the Ni-Co-ferrite obtained separately, as seen in Fig. 5a. On the other hand, it can be observed that the unit cell parameter of $BaTiO_3$ in the biphasic system, in all the compositions evaluated, did not show major changes when compared to its analog obtained separately. These results corroborated the fact that the two constituent phases of the system $BaTiO_3/0.2Ni_{(1-x)}Co_xFe_2O_4$ crystallized simultaneously and in an isolated form, ensuring the chemical integrity of each phase.

The BET specific surface area and the average particle diameter calculated for all nanopowders of the biphasic $0.8BaTiO_3/0.2Ni_{(1-x)}Co_xFe_2O_4$ system, as well as the $Ni_{(1-x)}Co_xFe_2O_4$ obtained separately, are shown in Fig. 5b, according to Tables I and II. It can be observed that the surface area decreased with increasing molar concentration of cobalt in the $Ni_{(1-x)}Co_xFe_2O_4$ phase and there was a maximum value for the molar ratio 0.75Ni:0.25Co, which was the same behavior in the *in situ* biphasic system. This result ensured that the increase in the surface area of the ceramic powders both in the ferrite phase obtained separately and in the biphasic system obtained via *in situ* synthesis depended on the molar ratio between Ni^{2+} and Co^{2+}.

From the results of the EDX analysis performed in order to quantitatively determine the elemental chemical composition of the nanopowders obtained from the biphasic system $0.8BaTiO_3/0.2Ni_{(1-x)}Co_xFe_2O_4$, presented in Table III, it was observed that the relationships between the experimental and theoretical molar values were very similar

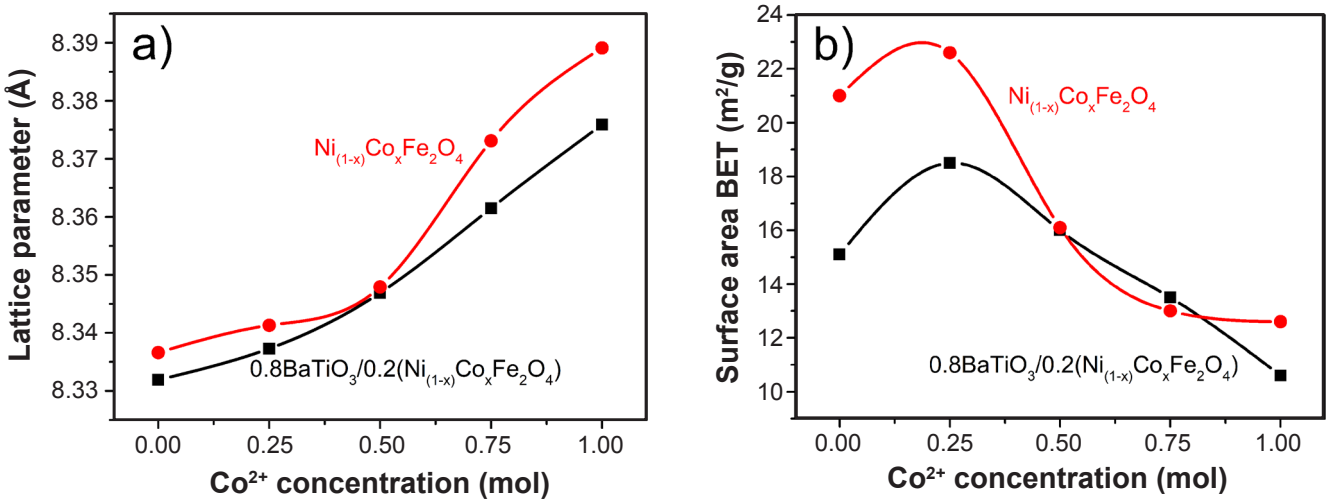

Figure 5: Variation of lattice parameter (a) and specific surface area (b) as a function of cobalt concentration in the *in situ* synthesized $0.8BaTiO_3/0.2Ni_{(1-x)}Co_xFe_2O_4$ and $Ni_{(1-x)}Co_xFe_2O_4$ phase obtained separately. All powders were heat-treated at 800 °C for 1 h.

Table III - EDX results of $0.8BaTiO_3/0.2Ni_{(1-x)}Co_xFe_2O_4$ nanopowders synthesized at 800 ºC for 1 h.

Element	Composition x (mol)									
	0		0.25		0.50		0.75		1.00	
	RE (mol%)	RT (mol%)	RE (mol%)	RT (mol%)	RE (mol%)	RT (mol%)	RE (mol%)	RT (mol%)	RE (mol%)	RT (mol%)
Ba	56.97	60.28	56.12	60.28	57.61	60.28	56.97	60.28	56.70	60.28
Ti	21.53	21.01	23.12	21.01	21.44	21.01	21.84	21.01	22.34	21.01
Co	-	-	0.75	1.62	3.54	3.23	5.37	4.85	7.08	6.47
Ni	7.66	6.44	5.74	4.83	3.75	3.22	1.89	1.61	-	-
Fe	13.84	12.26	14.26	12.26	13.65	12.26	13.94	12.26	13.89	12.26

RE: experimental content; RT: theoretical content.

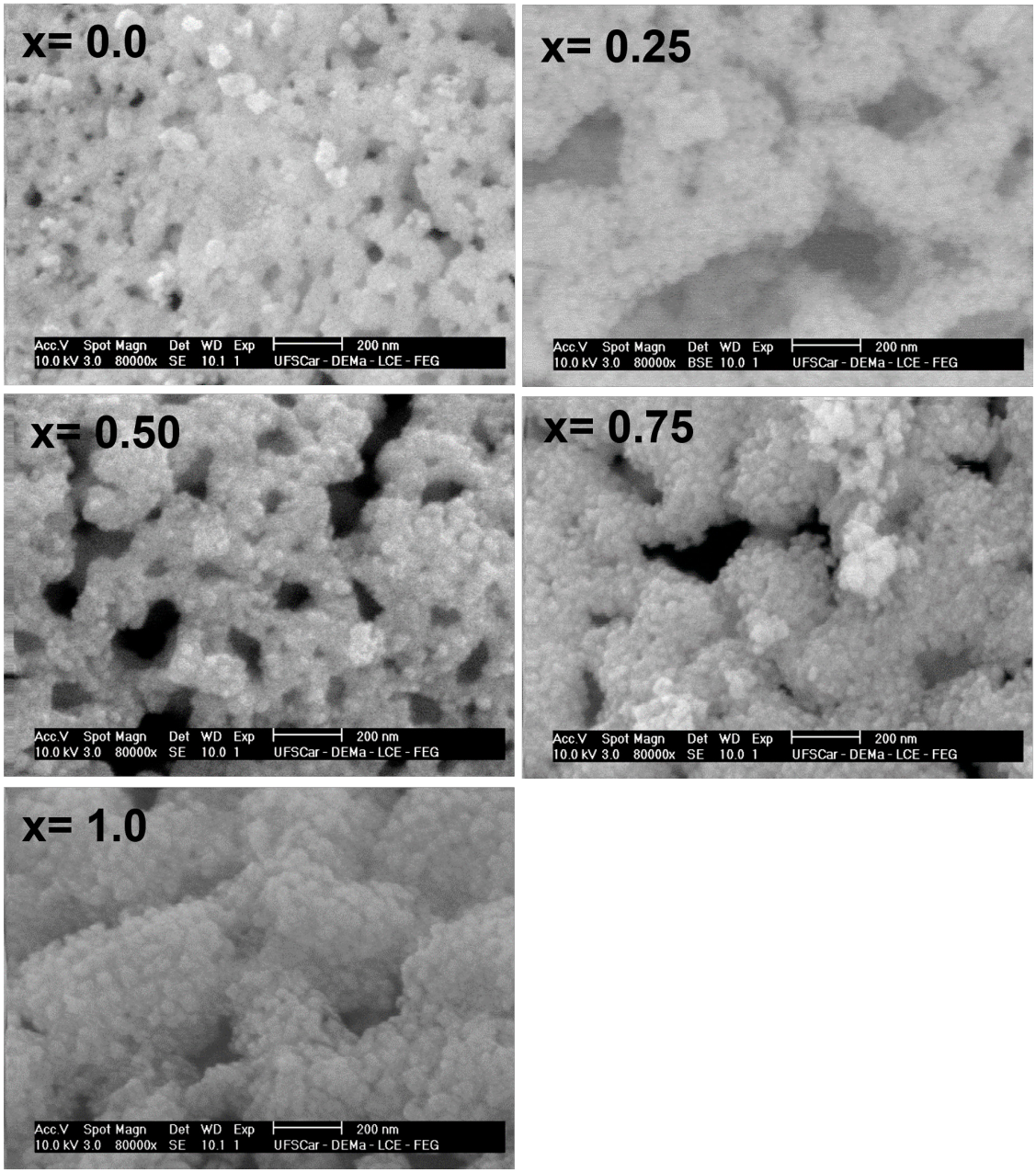

Figure 6: SEM micrographs of $0.8BaTiO_3/0.2Ni_{(1-x)}Co_xFe_2O_4$ nanopowders synthesized at 800 ºC for 1 h.

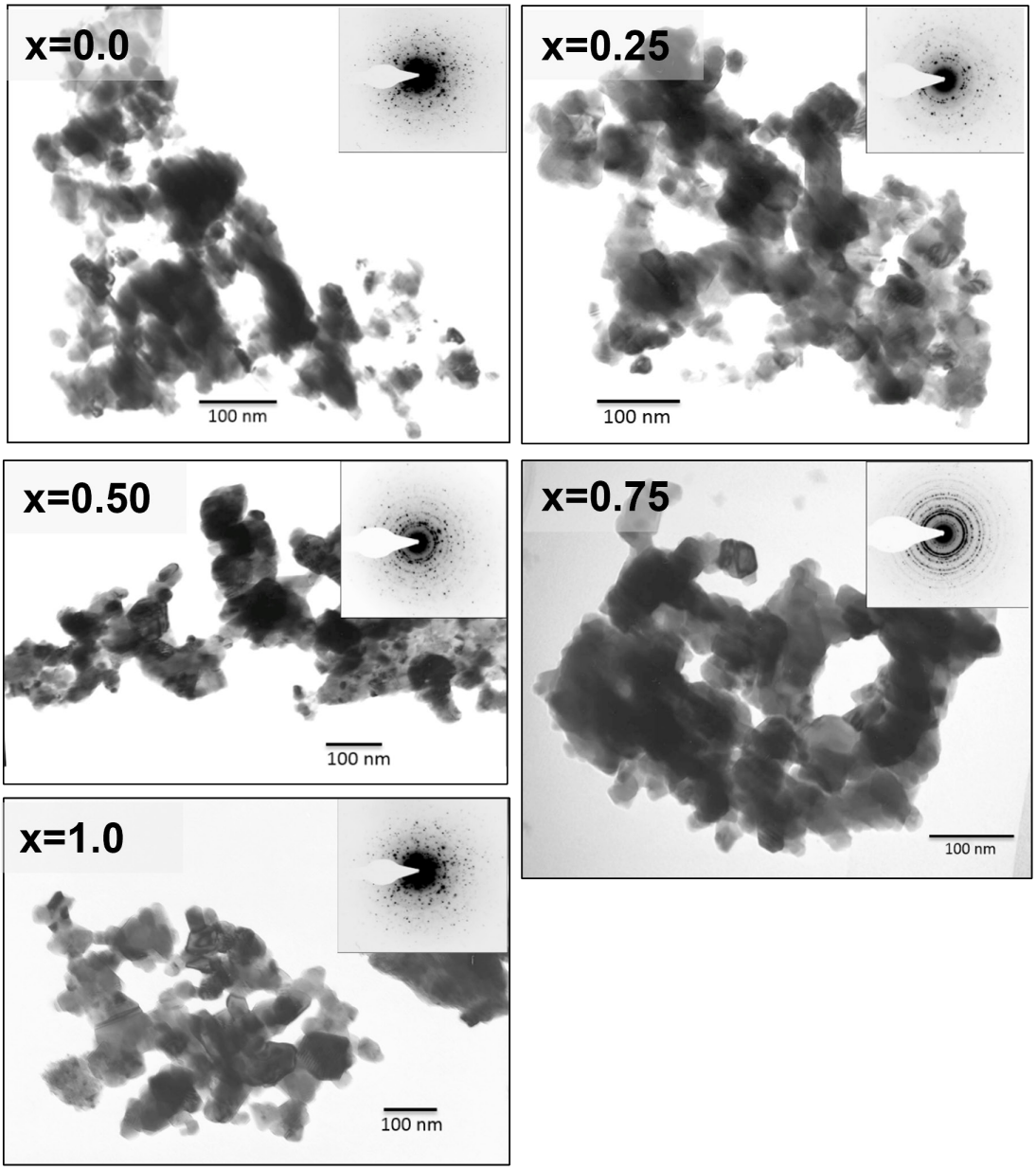

Figure 7: TEM micrographs of $0.8BaTiO_3/0.2Ni_{(1-x)}Co_xFe_2O_4$ nanopowders synthesized at 800 ºC for 1 h.

in all compositions synthesized and analyzed, corroborating the high efficiency of the *in situ* synthesis protocol by sol-gel used in this work.

SEM micrographs of $0.8BaTiO_3/0.2Ni_{(1-x)}Co_xFe_2O_4$ nanopowders synthesized at 800 ºC for 1 h are shown in Fig. 6. It can be observed the presence of easily pulverized agglomerates (high porosity), typical of the synthesis method, which were formed by primary particles of approx. size between 30 and 100 nm. The $0.8BaTiO_3/0.2Ni_{(1-x)}Co_xFe_2O_4$ nanopowders heat-treated at 800 °C for 1 h had a heterogeneous size distribution, as seen in the SEM micrographs of Fig. 6. It was determined that the agglomerates were made up of equiaxed primary particles with sizes between 20 and 100 nm, measured directly in brightfield TEM micrographs (Fig. 7) and in accordance with the size estimated by SEM (Fig. 6). The selected area electron diffraction (SAED) patterns included as inserts in the TEM micrographs (Fig. 7) showed a characteristic polycrystalline pattern, consisting of regular dots associated with large crystals, such as the compositions with low cobalt content (x=0.25) and the nanocrystalline pattern of the ring type for the compositions with cobalt content above 0.5 mol (x= 0.5, 0.75, and 1). This result indicated a difference in the particle size of the nanopowders of the biphasic system, corroborating the BET surface area results shown in Fig. 5, which was the decrease in surface area as a function of the increase in the concentration of Co^{2+} in Ni-ferrite. It is speculated that the PAA1800, used as the chelating agent in this work, may help to decrease the size of the ceramic powders obtained using the sol-gel method and is consistent with the results of other authors [18, 27].

CONCLUSIONS

Using the *in situ* sol-gel synthesis with poly(acrylic acid) (PAA1800) as the chelating agent, nanopowders of biphasic $0.8BaTiO_3/0.2Ni_{(1-x)}Co_xFe_2O_4$ (x= 0, 0.25, 0.5, 0.75, and 1) system were synthesized in a single step at a relatively low temperature (800 °C) and there was no evidence of phase interdiffusion as shown by XRD analysis. Depending on the cobalt content in the nickel ferrite phase, the specific surface area and the particle size of the nanopowders could be controlled. The *in situ* sol-gel synthesis used in this work provided an efficient and fast method for producing biphasic barium titanate/cobalt-nickel ferrite nanopowders with an average particle size of about 50 nm with a potential application in a lead-free magnetoelectric particulate composite.

ACKNOWLEDGMENTS

The authors gratefully acknowledge the financial support from the Brazilian agencies FAPESP (Proc. n. 2017/13769-1), and CNPq (Proc. n. 30129/2018-0). This study was financed in part by the Coordenação de Aperfeiçoamento de Pessoal de Nível Superior - Brasil (CAPES) - Finance Code 001.

REFERENCES

[1] Q. He, E. Arenholz, A. Scholl, Y.-H. Chu, R. Ramesh, Curr. Opin. Solid State Mater. Sci. **16**, 5 (2012) 216.
[2] X. Liang, H. Chen, N.X. Sun, APL Mater. **9** (2021) 41114.
[3] S.N. Achary, O.D. Jayakumar, A.K. Tyagi, in "Functional materials: preparation, processing and applications", S. Banerjee, A.K. Tyagi (Eds.), Elsevier (2012) 155.
[4] P. Chavan, L.R. Naik, R.K. Kotnala, J. Magn. Magn. Mater. **433** (2017) 24.
[5] Y. Kumar, K.L. Yadav, J. Mater. Sci. Mater. Electron. **29** (2018) 8923.
[6] Y. Zhou, J. Zhang, B. Li, Y. Su, B. Kang, S. Cao, Curr. Appl. Phys. **11** (2011) S232.
[7] S. Liu, L. Deng, S. Yan, H. Luo, L. Yao, L. He, Y. Li, M. Wu, S. Huang, J. Appl. Phys. **122** (2017) 34103.
[8] J.R. Munoz, E.R. Botero, D. Garcia, R.H.G.A. Kiminami, Ceram. Int. **45** (2019) 8593.
[9] M. Geramilla, R. Balakrishnan, S.T. Natarajan, M.S.R. Rao, Appl. Phys. A **125** (2019) 39.
[10] M. Etier, C. Schmitz-Antoniak, S. Salamon, H. Trivedi, Y. Gao, A. Nazrabi, J. Landers, D. Gautam, M. Winterer, D. Schmitz, H. Wende, V.V. Shvartsman, D.C. Lupascu, Acta Mater. **90** (2015) 1.
[11] R.C. Kambale, J. Alloys Compd. **489** (2010) 310.
[12] F.L Zabotto, A.J. Gualdi, P.C. de Camargo, A.J.A. de Oliveira, J.A. Eiras, D. Garcia, J. Alloys Compd. **676** (2016) 80.
[13] C.P. Fernández, F.L. Zabotto, D. Garcia, R.H.G.A. Kiminami, Ceram. Int. **43** (2017) 5925.
[14] C.P. Fernandez Perdomo, R.H.G. A Kiminami, D. Garcia, Ceram. Int. **45** (2019) 7906.
[15] A.L. Micheli, Ceram. Int. **15** (1989) 131.
[16] D. Chen, X. He, Mater. Res. Bull. **36** (2001) 1369.
[17] P.P. Hankare, K.P. Sanadi, K.M. Garadkar, D.R. Patil, I.S. Mulla, J. Alloys Compd. **553** (2013) 383.
[18] C.P.F. Perdomo, A.V. Suarez, R.F.K. Gunnewiek, R.H.G.A. Kiminami, J. Alloys Compd. **849** (2020) 156564.
[19] J.E. Elliott, M. Macdonald, J. Nie, C.N. Bowman, Polym. Int. **45** (2004) 1503.
[20] V. Kabanov, V. Dubnitskaya, S. Khar'kov, Polym. Sci. USSR **7** (1975) 1848.
[21] M. Dunuwille, C.S. Yoo, J. Chem. Phys. **139** (2013) 214503.
[22] F.V. Motta, A.P.A. Marques, M.T. Escote, D.M.A. Melo, A.G. Ferreira, E. Longo, E.R. Leite, J.A. Varela, J. Alloys Compd. **465** (2008) 452.
[23] X. Shen, Z. Zhou, F. Song, X. Meng, J. Sol-gel Sci. Technol. **53** (2010) 405.
[24] M.H. Frey, D.A. Payne, Chem. Mater. **7** (1995) 123.
[25] X. Xing, J. Deng, J. Chen, G. Liu, J. Alloys Compd. **384** (2004) 312.
[26] P.N. Kumar, S. Kannan, RSC Adv. **4** (2014) 29946.
[27] S. Mazumder, G.S. Bhattacharyya, Ceram. Int. **30** (2004) 389.

(Rec. 28/06/2021, Rev. 04/09/2021, Ac. 15/09/2021)